Formation Features of the Structure and Mechanical Properties in Rolled Products with Various Thicknesses from Low-Carbon Microalloyed Steel Produced at an Integrated Casting and Rolling Facility

V. V. Naumenko[a, b,]*, K. S. Smetanin[a,], A. V. Muntin[c,]***,
O. A. Baranova[a,]****, and S. V. Kovtunov[a,]*******

[a] Vyksa Steel Works, Vyksa, 607060 Russia
[b] Vyksa Branch, National University of Science and Technology—MISIS (NUST MISIS), Vyksa, 607036 Russia
[c] Bauman Moscow State Technical University, Moscow, 105005 Russia
*e-mail: naumenko_vv@vsw.ru
**e-mail: smetanin_ks@vsw.ru
***e-mail: muntin_av@omk.ru
****e-mail: baranova_oa@vsw.ru
*****e-mail: kovtunov_sv@omk.ru

Abstract—The article considers the results of studying the influence of the microstructural parameters of Charpy specimens with a sharp stress concentrator and Mesnager specimens with a circular stress concentrator from rolled products of various thicknesses on their impact strength at temperatures from 0 to −80°C with an increment step of 20°C. The used roll products were made from low-carbon microalloyed steel at JSC "Vyksa Steel Works". The tests were conducted using optical and scanning electron microscopy. It is shown that the thinner metal pieces (6 and 8 mm) have the same chemical composition and are treated in the same thermomechanical modes as their thicker counterparts but have higher strength properties (by 10 MPa on average for temporary resistance and by 30 MPa for yield strength) and a viscosity margin at negative temperatures at close grain score values and average grain size corresponding to numbers 10−11 according to GOST 5639. The lowest level of cold resistance is shown by the metal pieces with a thickness of 12 mm, and their brittle transition temperature is -50°C. The structure of the rolled products of various thicknesses exhibits variations in grain size. The thinner rolled products contain smaller grains corresponding to number 14. The thicker rolled products contain larger grains corresponding to number 8. The electron microscopic examination by the Electron Backscatter Diffraction (EBSD) technique helps find out that the rolled products of 6 and 8 mm in thickness contain more high-angle boundaries, which are barriers for brittle cracking. The constructed orientation maps of microstructure reveal the presence of pronounced strain texture corresponding to orientations $\langle 110 \rangle \parallel$ RD (rolling direction) and $(\langle 113 \rangle...\langle 112 \rangle) \parallel$ RD for the rolled products with a thickness of 6 mm.

Keywords: structural steel, integrated casting and rolling facility, microstructure, mechanical properties, impact strength, electron backscatter diffraction, crystallographic orientation, small- and large-angle boundaries

DOI: 10.3103/S0967091221090096

INTRODUCTION

The integrated casting and rolling facility (ICRF) of JSC Vyksa Steel Works makes coiled stock of 1 to 2.7 mm in thickness from various steels by combining smelting, teeming, direct rolling with rapid cooling and reeling [1−5]. The most popular thickness range of metals used in making electric-welding pipes for oil and gas industries is from 5 to 12.7 mm [6].

A metal with a single chemical formula has traditionally been endowed with various chemical properties by thermal mechanical processing (TMP) in different modes, followed by cooling needed to form different structural states in the metal [7−15]. However, the coiled stock of 5 to 12.7 mm in thickness made using the single technology (chemical composition and TMP modes) at the ICRF can exhibit significant differences in mechanical properties, the most pronounced of which is impact viscosity.

According to the previous studies, the tendency during the dynamic impact bending tests of Sharpy

and Mesnager specimens of coiled stock of various thicknesses was as follows: the smaller was the ultimate rolled thickness, the lower were the temperatures at which the metal was exposed to ductile fracture. For example, the coiled stock of 5 to 9 mm in thickness appears to have a cold resistance margin in comparison with the thicker rolled stock of 10 to 12.7 mm. In that case, the grain number under GOST 5639 and the average ferrite grain size were sufficiently close in value.

Based on the foregoing, the goal of the work was to study the influence of structural factor on the cold resistance of the coiled stock of various thicknesses made at the ICRF.

MATERIALS AND METHODS

The material used in the study was the low-carbon microalloyed steel coiled stock with a thickness of 6, 8, 10, and 12 mm made at the ICRF. The steel was smelted in an electric-arc furnace, exposed to ladle refining, teemed by continuous casting to a slab of 105 mm in thickness, heated in a tunnel furnace to the preset temperature and rolled on a continuous hot strip mill 1950 in two stages: first, it was rolled in two stands of the roughing mill; then, it was rolled in six stands of the finishing mill group. After the rolling, the breakdown bars were rapidly cooled and coiled. The coiled stock of various thicknesses is made in various TMP modes with the strain finishing in the lower temperature range of the austenitic region. Whatever the thickness, the stock was characterized by similar temperature parameters of strain in both TMP stages, rapid afterstrain cooling and coiling conditions.

The chemical composition of the metal in % was as follows: ≤0.07 of C; ≤1.5 of Mn; ≤0.05 of Si; ≤0010 of P; ≤0.005 of S; ≤0.008 of N; ≤0.035 of Nb and other nonferrous impurities from the charge (Cr, Ni, Cu).

The mechanical properties of the studied metal exposed to static tension tests and dynamic impact bending tests were estimated on the specimens cut out lengthwise and edgewise relative to the rolling direction. The static tension tests were conducted under GOST 1497 on flat quintuple full-thickness specimens and helped define ultimate tensile resistance σ_{ts} (N/mm^2), yield strength σ_Y (N/mm^2), and percentage elongation σ_5 (%). The Sharpy and Mesnager specimens were exposed to dynamic impact bending tests under GOST 9454 every 20°C at temperatures from 0 to −80°C. Ten specimens were tested at each of the chosen temperatures, which included the reading of impact viscosity values (KCV, KCU, J/cm^2) during each test. The respective thicknesses of the impact specimens from the rolled stock of 12, 10, and 8, and 6 mm were 10, 7.5, and 5 mm.

The structural state of the metal was studied by the metallographic method and electron microscopy on polished specimens made lengthwise relative to the rolling direction. The metallographic test of the structure after the chemical etching of the polished specimens in the 4% alcoholic solution of nitrogen acid was conducted using a coded optical microscope Axio Observer D1m with a Thixomet Pro image analysis system.

The electron microscopic examination of the structure was made on unetched polished specimens by the EBSD Technique with the help of an Ultra-55 scanning electron microscope. The maps of crystallographic orientations of crystallites in the Euler space were drawn using the Oxford Instruments HKL Channel 5 system of analyzing electron backscattered diffraction [16, 17]. The orientation maps were drawn lengthwise at a depth of 1/4 rolled thickness at magnifications of 125, 500, and 1500 with a respective step of 500, 200, and 80 nm. The respective areas of the scanned regions were 928 × 696, 232 × 174, and 77 × 58 μm. The larger side of the map is parallel to the rolling direction (RD) and perpendicular to the normal line (NL) to the rolling plane. The orientation maps were automatically modified for reducing the number of nondisplayed and improperly displayed data before the quantitative estimation of the microstructural parameters.

All of the low-angle boundaries (LABs) among the kernel volumes with a misorientation below 2° were excluded from consideration due to the experimental error of the EBSD technique. Crystallite misorientation angle θ of 15° was used as the LAB-HAB differentiation criterion. Thus, the LABs on the EBSD maps were drawn in a misorientation angle range of $2° \leq \theta < 15°$, whereas the high-angle boundaries were drawn at $\theta \geq 15°$. The quantitative evaluation of the LABs and HABs was made by defining grain boundary density ρ_b in μm^{-1} by formula (1) for each type of crystallite misorientation:

$$\rho_b = \frac{L_b}{S}, \qquad (1)$$

where L_b is the total length of the grain boundaries, μm; S is the analysis area, μm^2.

The substructure of the test steels was evaluated for comparison by drawing Kernel Average Misorientation (KAM) maps on the basis of the EBSD data. These maps characterize the spatial distribution of microstresses and strains in the examined material. The growing density of mislocations and the rising level of microstresses increase the kernel misorientation of the crystalline lattice. Kernel misorientation maps are drawn as described below. The average misorientation relative to the nearest neighboring points is defined for each point on the EBSD map, and this value is attached to the initial pixel and shown in a certain color in the chosen color scheme. Misorientation maps are designed considering angles with less defined values, which is done to avoid the influence of high-angle boundaries. In this work, the angle of 5° was set

as the criterion for processing the EBSD maps. Each pixel on the map was assigned with a defined color smoothly changing from red to dark blue; the color characterized the kernel misorientation value. The pixels with a kernel misorientation of 5° were shown in red. The pixels with zero misorientation values were shown in blue.

The crystallographic texture in the examined coiled stock was estimated using the orientation distribution function (ODF) represented as the 3D distribution of Euler angles of orientation density $F(\varphi_1, \Phi, \varphi_2)$ by the Bunge method. The ODF was drawn using the Oxford Instruments Channel 5 software suite on the basis of the data of fixed EBSD maps. The crystallographic texture analysis was made by the conventional method for cubic crystals by 2D ODF section at angle $\varphi_2 = 45°$. This section is the one, where most of the orientations typical of strain textures and recrystallization of VCCL and FCC metals are located (Fig. 1) [18−20]. In the 2D ODF section, the horizontal legs correspond to certain crystallographic planes {hkl}, whereas the points of these sections correspond to crystallographic directions ⟨uvw⟩ within these planes.

Fig. 1. Positions of ideal orientations on the 2D sections of the orientation distribution function according to the Bunge method at angle $\varphi_2 = 45°$.

RESULTS AND DISCUSSION

As shown by the microstructural examination of the coiled stock by optical microscopy, the TMP and rapid cooling of the metal of various thicknesses (6, 8, 10, and 12 mm) was attended by the generation of a ferrite-perlitic structure with a perlite content of no more than 3% (Fig. 2). As shown by estimating the ferrite grain size under GOST 5439, all of the examined specimens had similar grain sizes corresponding to number 10−11 at nonhomogeneity numbers from 9 to 14. In the rolled stock with a thickness of 6, 8, and 10 and 12 mm, the respective nonhomogeneity numbers were 10 to 14, 9 to 13, and 8 to 13.

As shown by the static tension test results, the coiled stock with a thickness of 6 and 8 mm has better strength properties and poorer plastic properties than the coiled stock of 10 and 12 mm in thickness (Table 1).
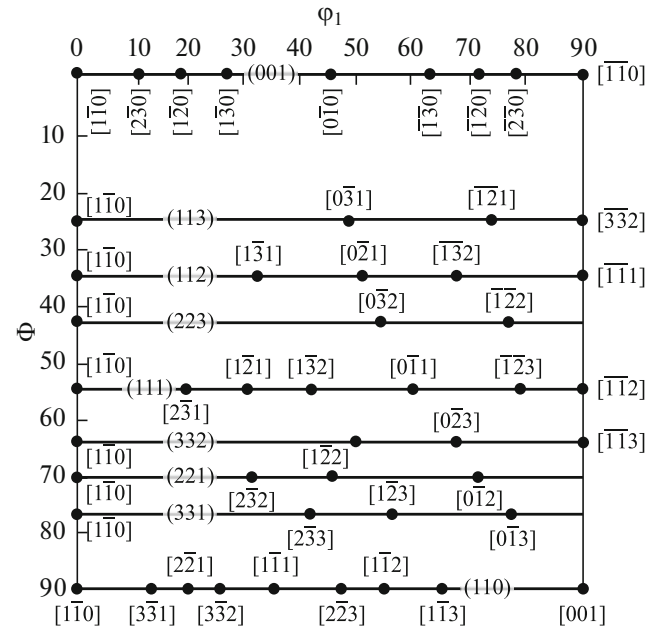
The temporary lengthwise and edgewise resistance of the specimens is higher by 10 to 15 mPa on average. The lengthwise and edgewise yield stresses is higher by 30 mPa on average. The percentage elongation is shorter by 2 to 3%.

The resulting strength properties can point to the fact that the presence of finer ferrite grains in the coiled stock of 6 and 8 mm in thickness can possibly contribute to the grain-boundary hardening of the metal, which helps obtain higher strength levels in the metal of the smaller thickness.

For the results of the dynamic impact bending tests, see Figs. 3 and 4. It is clearly seen that the specimens from the coiled stock of various thicknesses exhibit similar types of impact viscosity relations;

Table 1. Mechanical properties of the rolled product

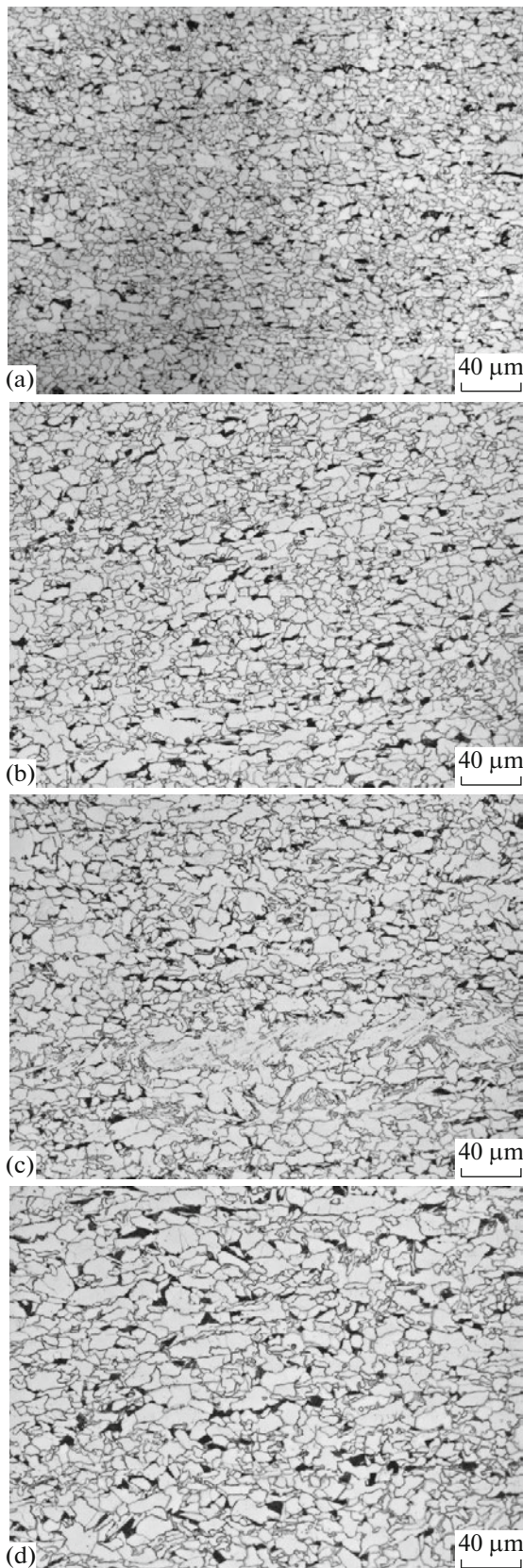| Thickness, mm	Temporary resistance, mPa		Yield strength, mPa		percent elongation, %	
	edgewise	lengthwise	edgewise	lengthwise	edgewise	lengthwise
6	510−528 / 518	496−523 / 510	429−448 / 442	417−443 / 429	32.0−35.0 / 34.5	33.0−45.0 / 37.5
8	509−520 / 517	501−517 / 512	417−445 / 438	424−432 / 427	32.0−37.0 / 35.1	33.0−40.0 / 36.6
10	499−513 / 506	495−505 / 499	397−422 / 409	396−413 / 401	35.0−39.0 / 36.4	32.0−40.0 / 37.8
12	505−514 / 509	489−502 / 496	399−415 / 408	388−405 / 395	37.0−40.0 / 38.9	37.0−44.0 / 40.7

Fig. 2. Microstructure of the tested metal per 1/4 of the rolled thickness of 6 (a), 8 (b), 10 (c), and 12 mm (d).
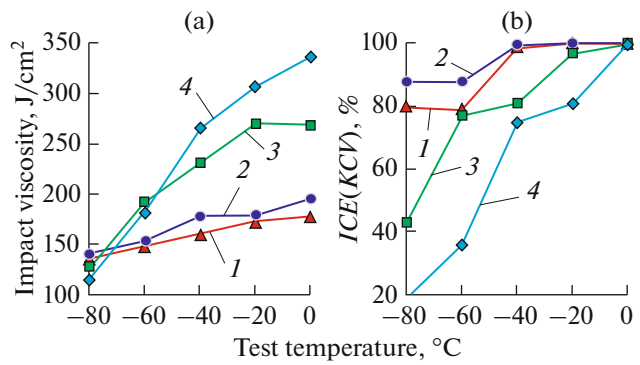

Fig. 3. Dependence of the impact strength (a) and proportion of the viscous component (b) of the Charpy specimens on the test temperature for the rolled product of 6 (*1*), 8 (*2*), 10 (*3*), and 12 mm (*4*) in thickness.
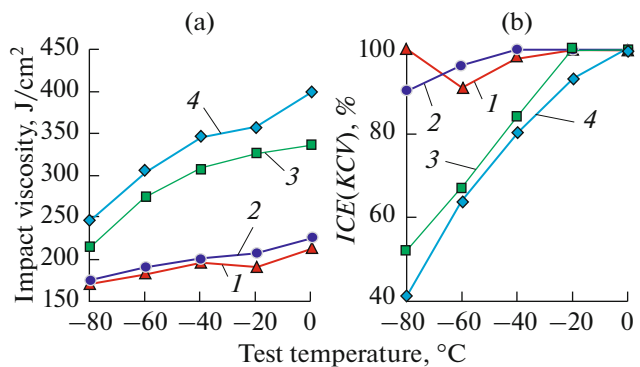

Fig. 4. Dependence of the impact strength (a) and proportion of the viscous component (b) of the Mesnager specimens on the test temperature for the rolled product of 6 (*1*), 8 (*2*), 10 (*3*), and 12 mm (*4*) in thickness.

however, the values proper are characterized by considerable differences in the impact viscosity levels.

Ductile-brittle transition temperature T_{50} of the edgewise Sharpy specimens from the coiled stock with a thickness of 6 and 8 mm is below −80°C, whereas respective T_{50} of the coiled stock with a thickness of 10 and 12 mm is −75 and −50°C.

Thus, as shown by the dynamic impact bending tests of the Sharpy and Mesnager specimens, the coiled stock of 6 and 8 mm in thickness exhibits the highest cold resistance margin because the temperatures (T_{50}), at which the transition to brittle fracture occurs in this metal, are lower than in the coiled stock with a thickness of 10 and 12 mm. The strongest tendency to brittle fracture is exhibited by the coiled stock with a thickness of 12 mm, which has to do with the features of its structural state, in particular, with the presence of larger ferrite grains.

As shown by examining the microstructure represented as Kikuchi lines, the main structural component of all of the examined specimens is polygonal fer-
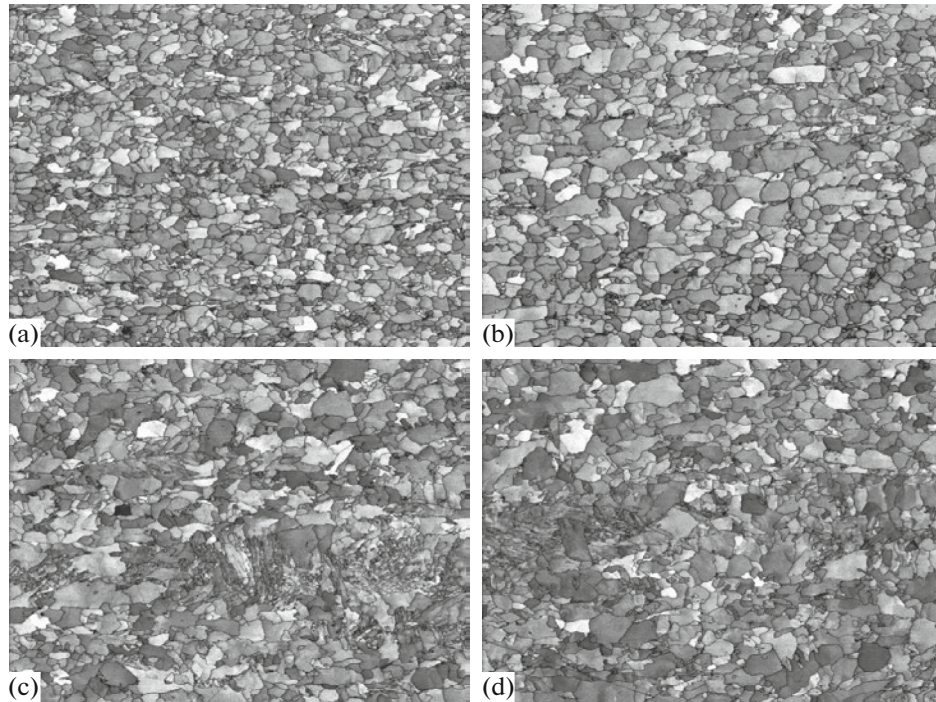
Fig. 5. Contrast maps of Kikuchi-paintings per 1/4 of the tested rolled product thickness of 6 (*1*), 8 (*2*), 10 (*3*), and 12 mm (*4*) in thickness.

rite (Fig. 5). The coiled stock of 6 and 8 mm in thickness contains thin strips which stretch along the RD and consist from quasi-polygonal ferrite grains and acicular bainite. The coiled stock with a thickness of 10 and 12 mm contains coarse extended sections consisting mainly from bainite of various morphologies and quasi-polygonal ferrite. The maximal respective length and width of those sections in the examined vision fields were about 500 and 50 μm.

It is known that the mechanical properties of metal are largely defined by the amount of boundaries [21−23]. The denser are the boundaries, the smaller is the effective grain size on which the strength, viscosity, and cold resistance of steel depend. Note that

LABs inhibit the motion of dislocations and favor strength improvement but do not inhibit the propagation of brittle cracks that is inhibited only by high-angle boundaries.

The grain size of the examined steels was estimated by processing the EBSD maps; it was taken that the boundaries with a minimal misorientation of 15° were high-angle boundaries. For the bar graphs that result from the analysis and show the grain distribution by size, including average (D_{avg}) and average weighted ($D_{av.wt}$) size, see Fig. 6.

For the quantitative characteristics of the rolled stock structure, see Table 2.

Table 2. Characteristics of the rolled product structure obtained by analyzing the EBSD maps

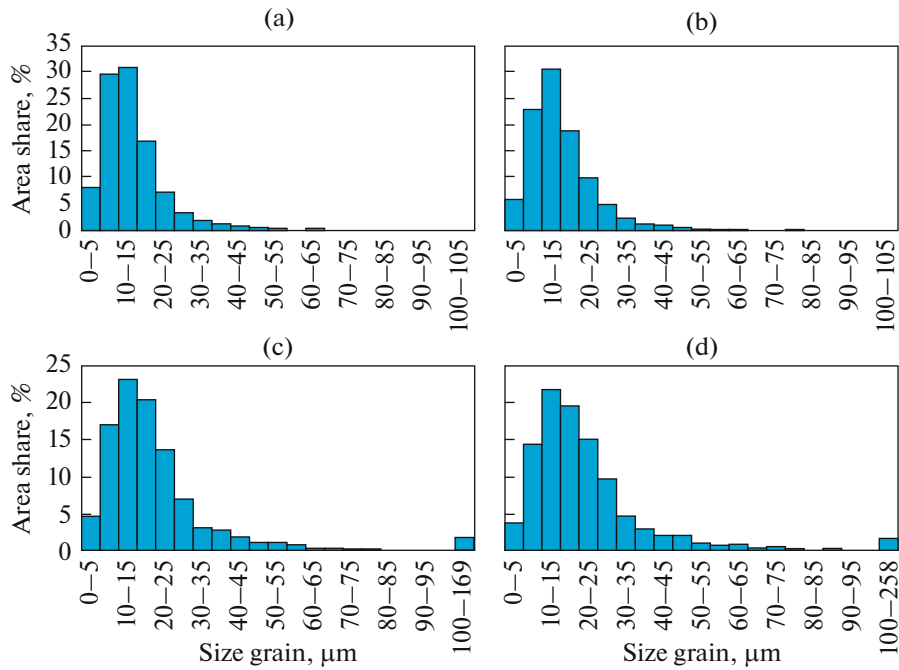| Index	Rolled product thickness, mm			
	6	8	10	12
Average Feret diameter D_{avgp}, μm	6.4	6.7	7.6	8.2
Maximum Feret size D_{max}, μm	63.1	76.9	168.2	257.6
Average weighted Feret size $D_{avg. wt}$, μm	13.3	15.2	21.2	22.8
Average grain area S_{avg}, μm^2	24.7	30.8	37.2	44.0
Maximum grain area S_{avg}, μm^2	565.3	1170.0	4813.3	7260.5
Grain number by average diameter G (d_{avg})	11.6	11.4	11.1	10.8
Grain number by average area G (S_{avg})	12.3	12.0	11.7	11.5
Grain number by average weighted diameter G ($d_{avg. wt}$)	9.9	9.6	8.9	8.7
Grain diameter variation coefficient, %	81.2	86.2	90.8	86.4
Nonhomogeneity ratio K_{nhg}	5.0	6.2	13.5	20.6

Fig. 6. Bar graphs of the grain size distribution for the rolled product thickness of 6 (*1*), 8 (*2*), 10 (*3*), and 12 mm (*4*).
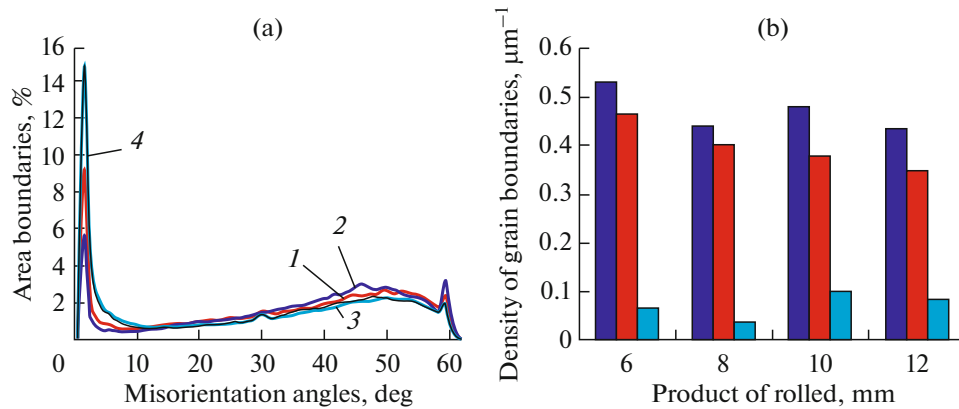

Fig. 7. Frequency distributions of the crystallite misorientation angles (a) and the density of grain boundaries (b) in the tested rolled product of 6 (*1*), 8 (*2*), 10 (*3*), and 12 mm (*4*) in thickness; (■) the high + low-angle boundaries are shown in dark blue; (■) the high-angle boundaries are in red; (■) the low-angle boundaries are in blue.

The examined steels have a fairly close average grain size of 6.4 to 8.2 μm. However, the bar graphs of the grain distribution by size clearly show that, with an increase in the rolled thickness, the distribution peak shifts to the region of higher values, the distribution becomes broader and more asymmetrical (Fig. 6). Taking this into consideration, it is more correct to compare average weighted grain diameters and necessary to evaluate the structure for nonhomogeneity.

With the coiled stock thickness rising from 6 to 12 mm, the average weighted grain size rises from 13.3 to 22.8 μm. The longer $D_{av.wt.}$ in the coiled stock of 8 mm in thickness compared with the coiled stock of

6 mm in thickness is conditioned by the formation of larger ferrite grain, which is clearly seen in the structural comparison in Fig. 5.

In addition to the growing ferrite grain size, the coiled stock of 10 and 12 mm in thickness is characterized by the formation of coarse bainitic areas in its structure, and the length of these areas can reach several hundreds of micrometers. Since the boundaries inside the bainitic colonies are mostly low-angle, the effective bainite grain size is commensurate with the size of the bainite areas proper and reaches about 170 μm in the coiled stock of 10 mm in thickness and
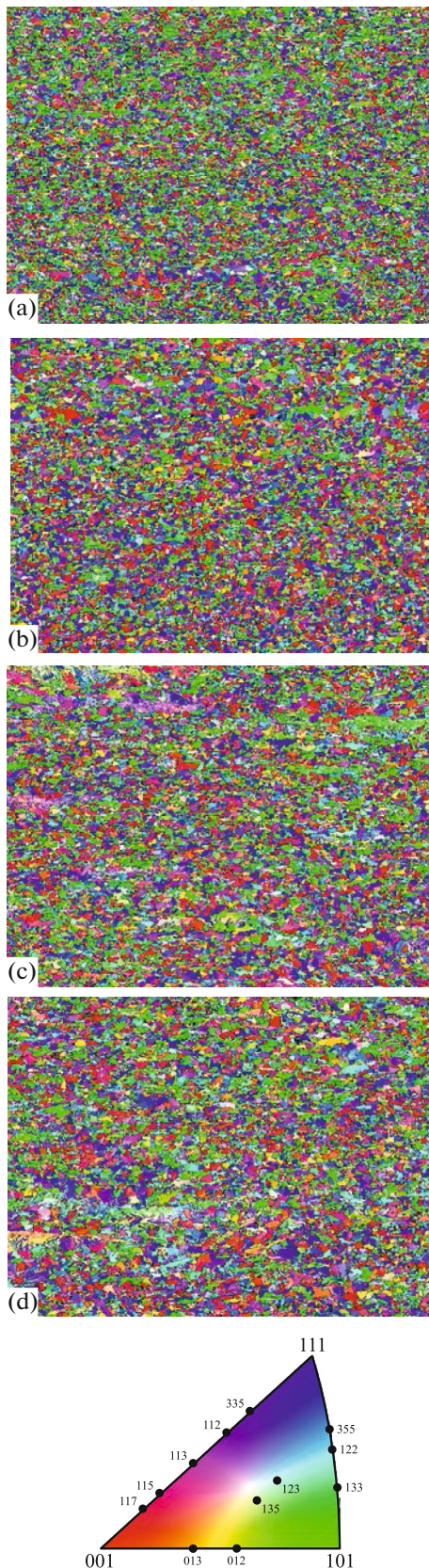
Fig. 8. Orientation microstructural maps of the studied rolled products in the color scheme of a standard stereographic triangle for the rolling direction.

about 260 μm in the coiled stock of 12 cm in thickness (Fig. 6).

The structural nonhomogeneity of the metal can be evaluated using parameter K_{nh} defined as the relation of the maximal effective grain size to the size of the grains covering the largest area on the polished specimen. The coiled stock of 10 and 12 mm in thickness with K_{nh} of 13.5 to 20.6 contains large bainite areas, which is why this stock is very different in K_{nh} from the thinner metal with $K_{nh} = 5.0-6.2$ (Table 2).

For the frequency distributions of crystallite misorientation angles and the results of estimating the grain boundary densities, see Fig. 7. It is easy to see that, with an increase in the rolled thickness, the fraction and density of HABs decrease through the growth of the ferrite grains and generation of coarse bainitic areas in the structure. On the contrary, the amount of LABs is much higher in the specimens with a thickness of 10 and 12 mm than in the stock of 6 and 8 mm in thickness.

For the orientation maps of the microstructure of the examined stock in the color scheme of a standard stereographic triangle for the RD, see Fig. 8. It is seen that open texture is characteristic only of the coiled stock of 6 mm in thickness: in the orientation map the dominant colors are green and purple corresponding to orientations $\langle 110 \rangle \parallel$ RD and $(\langle 113 \rangle ... \langle 112 \rangle) \parallel$ RD.

It is hard to distinguish dominant orientations on the orientation maps of the other specimens, which points to the generation of feeble crystallographic structure in the coiled stock of 8, 10, and 12 mm in thickness.

CONCLUSIONS

The picture revealed by the tests conducted as part of this study is considered below.

The rolled stock of 6 and 8 mm in thickness has better strength properties than the coiled stock of 10 and 12 mm in thickness (by 10 MPa on average for temporary resistance and by 30 MPa for yield strength).

As shown by the dynamic impact bending tests of Sharpy and Mesnager specimens, the thinner is the stock, the flatter is the impact viscosity—test temperature dependence curve. The rolled stock of 6 and 8 mm in thickness exhibits a better cold resistance characterized by the ductile-brittle transition temperature (T_{50}) (T_{50} is below −80°C). The rolled stock of 12 mm in thickness exhibits the lowest cold resistance ($T_{50} = -50$°C).

The average ferrite grain size estimated by the grain number under GOST 5639 is similar in the rolled stock of various thicknesses and corresponds to numbers 10−11. In this case, there is a spread in grain sizes. The thinner rolled stock contains smaller grains corre-

sponding to number 14, whereas the thicker rolled stock contains bigger grains corresponding to number 8.

As shown by estimating the grain size by processing the EBSD maps, the rolled stock of 10 and 12 mm in thickness has a lower fraction and density of HABs than the rolled stock of 6 and 8 mm in thickness because the former rolled stock contains coarse bainite sections with mainly LABs.

The orientation maps of the microstructure of the tested rolled stock have shown that the pronounced strain texture is characteristic only of the rolled stock of 6 mm in thickness. The rolled stock of 8, 10, and 12 mm in thickness has a feeble crystallographic texture.

The high brittle fracture resistance of the rolled stock of 6 mm in thickness at subzero temperatures is defined by the high cumulative plastic strain in its austenite at rolling and has to do with the presence of finer ferrite grain separated by HABs as well as by the formed strain texture corresponding to orientation $\langle 110 \rangle \parallel$ RD and $(\langle 113 \rangle ... \langle 112 \rangle) \parallel$ RD.

REFERENCES

1. Efron, L.I., *Metallovedenie v "bol'shoi" metallurgii. Trubnye stali* (Metal Science in "Great" Metallurgy. Pipe Steels), Moscow: Metallurgizdat, 2012.
2. Kislitsa, V.V., Lamukhin, A.M., Isaev, O.B., et al., Foundry and rolling complex: new technologies in the production of rolled products for pipe purposes, *Chern. Metall., Byull. Nauchno-Tekh. Ekon. Inf.*, 2013, no. 4, pp. 50−56.
3. Naumenko, V.V., Bagmet, O.A., Matrosov, M.Yu., Muntin, A.V., Kichkina, A.A., and D'yakonov, D.L., The influence of a microalloying system on the structure of a coiled strip produced under conditions of endless strip production, *Steel Transl.*, 2020, vol. 50, no. 7, pp. 501−508. https://doi.org/10.3103/S0967091220070104
4. Naumenko, V.V., Bagmet, O.A., and Mursenkov, E.S., Assimilation of production under casting and rolling conditions of pipe rolled product from steels of the V−N microalloying system resistant to cold and hydrogen sulfide cracking, *Metallurgist*, 2019, vol. 63, nos. 1−2, pp. 163−175. https://doi.org/10.1007/s11015-019-00806-x
5. Lamukhin, A.M. and Dubinin, I.V., Startup of a casting-rolling complex and mastery of the production of high-quality rolled products for electric-welded pipes, *Metallurgist*, 2020, vol. 54, nos. 1−2, pp. 19−27. https://doi.org/10.1007/s11015-010-9268-3
6. Chervonnyi, A.V., Ringinen, D.A., Chastukhin, A.V., Efron, L.I., Muntin, A.V., Naumenko, V.V., and Bagmet, O.A., Structure and property formation for pipe coiled rolled product during manufacture under casting and rolling complex conditions, *Metallurgist*, 2019, vol. 62, nos. 9−10, pp. 1012−1021. https://doi.org/10.1007/s11015-019-00748-4
7. Schwinn, V., Schuetz, W., Fluess, P., and Bauer, J., Prospects and state of the art of TMCP steel plates for structural and linepipe applications, *Mater. Sci. Forum*, 2007, vols. 539−543, part 5, pp. 4726−4731. https://doi.org/10.4028/www.scientific.net/MSF.539-543.4726
8. Hara, T., Shinohara, Y., Terada, Y., Asahi, H., and Doi, N., Metallurgical design and development of high deformable high strength line pipe suitable for strain-based design, *Proc. Int. Offshore and Polar Engineering Conf., Osaka, Japan, June 21−26, 2009*, Osaka, 2009, pp. 73-79.
9. DeArdo, A.J., Fundamental metallurgy of niobium in steel. Development and production of high strength pipeline steels, *Proc. Int. Symp. Niobium 2001, Orlando, USA, December 2−5, 2001*, Bridgeville, PA: Niobium-2001, 2001, pp. 427-500.
10. DeArdo, A.J., Producing high quality niobium-bearing steels using the CSP process at Nucor steel Berkeley, *Proc. 5th Int. Conf. HSLA Steels 2005, Sanya, Hainan, China, November 8−10, 2005*, Hainan, 2005, vol. 40, pp. 23−29.
11. Hillenbrand, H., Gras, M., and Kalwa, C., Development and production of high strength pipeline steels, *Proc. Int. Symp. Niobium 2001, Orlando, USA, December 2−5, 2001*, Bridgeville, PA: Niobium-2001, 2001, pp. 543-569.
12. Schwinn, V., Fluess, P., and Bauer, J., Production and progress of plates for pipes strength level of X80 and above, *Proc. Pipe Dreamers Conf.*, Yokohama, 2002, pp. 98−114.
13. Windhager, M., Kneissl, A., and Jeglitsch, F., Evolution of microstructure during the thermomechanical processing of HSLA steels, *Proc. Int. Symp. on Processing, Microstructure and properties of HSLA Steels, November 3−5, 1987*, Pittsburgh, PA, 1987, pp. 105-116.
14. Zhang, X., Yang, C., and Shang, C., New development of HSLA steels in China, in *HSLA Steels 2015, Microalloying 2015 & Offshore Engineering Steels 2015*, Cham: Springer-Verlag, 2015, pp. 3−15. https://doi.org/10.1002/9781119223399.ch1
15. Yang, C., R&D application of V-N microalloyed steels in China, in *HSLA Steels 2015, Microalloying 2015 & Offshore Engineering Steels 2015*, Cham: Springer-Verlag, 2015, pp. 917−930. https://doi.org/10.1002/9781119223399.ch115
16. Bagmet, O.A., Naumenko, V.V., and Smetanin, K.S., A study of the cold resistance of coiled stock for pipes produced at foundry rolling works. Part 1, *Met. Sci. Heat Treat.*, 2018, vol. 59, nos. 9−10, pp. 551−555. https://doi.org/10.1007/s11041-018-0188-3
17. Kolbasnikov, N.G., Zotov, O.G., Shamshurin, A.I., and Luk'yanov, A.A., Study of lath morphology bainite in high-strength pipe steel, *Met. Sci. Heat Treat.*, 2013, vol. 55, nos. 5−6, pp. 287−293. https://doi.org/10.1007/s11041-013-9621-9
18. Lobanov, M.L., Yurovskikh, A.S., Kardonina, N.I., et al., *Metody issledovaniya tekstur v materialakh* (Study Methods of Textures in Materials), Yekaterinburg: Ural. Fed. Univ., 2014.
19. Umanskii, Ya.S., *Kristallografiya, rentgenografiya i elektronnaya mikroskopiya* (Crystallography, Radiogra-

phy, and Electron Microscopy), Moscow: Metallurgiya, 1982.

20. Platov, S.I., Krasnov, M.L., Urtsev, N.V., Danilov, S.V., and Lobanov, M.L., Structural and textural states of steel 06G2MB strips after controlled thermomechanical treatment, *Met. Sci. Heat Treat.*, 2020, vol. 62, nos. 1−2, pp. 55−60.
https://doi.org/10.1007/s11041-020-00512-5

21. Joo, M.S., Suh, D.W., Bae, J.H., and Bhadeshia, H.K.D.H., Role of deamination and crystallography on anisotropy of Charpy toughness in API-X80 steel, *Mater. Sci. Eng., A*, 2012, vol. 546, pp. 314−322.
https://doi.org/10.1016/j.msea.2012.03.079

22. Haskel, H.L., Pauletti, E., Martins, J.P., and Carvalho, A.L.M., Microstructure and microtexture assessment of delamination phenomena in Charpy impact tested specimens, *Mater. Res.*, 2014, vol. 17, no. 5, pp. 1238−1250.
https://doi.org/10.1590/1516-1439.268314

23. Misra, R.D.K., Nathahi, H., Siciliano, F., and Carneiro, T., Effect of texture and microtexture on resistance to cracking of high-strength hot-rolled Nb−Ti microalloyed steels, *Metall. Mater. Trans. A*, 2004, vol. 35, pp. 3024−3029.

Translated by S. Kuznetsov